RESEARCH ARTICLE

NANO · MICRO small
www.small-journal.com

# Kinetic Insights into the Supramolecular Polymerization of Perylenediimide-Appended Dipeptides

*Francisco Rey-Tarrío, Carmen Atienza, and Luis Sánchez**

**This study describes the synthesis of two amphiphilic perylenediimide (PDI)-based systems, each incorporating lateral non-polar side chains and dipeptide units: (*L*)-Ala-Gly (PDI 1) or Gly-(*L*)-Ala (PDI 2). These amphiphilic dipeptide-functionalized systems enable the investigation of their self-assembly behavior in both apolar (MCH) and aqueous environments. The incorporation of dipeptides facilitates the formation of metastable monomeric species, *M**, which have been examined through experimental and theoretical approaches. Spectroscopic analysis reveals that these monomeric species adopt various configurations stabilized by intramolecular hydrogen bonding, forming pseudocycles of varying sizes. DFT calculations suggest that the metastable monomers and their unbonded forms possess similar stabilities, allowing them to coexist in solution. Interestingly, unlike other amino acid-based scaffolds, the presence of these metastable species does not lead to pathway complexity. Instead, a single H-type aggregate species emerges, driven by $\pi$-stacking of the PDI cores and intermolecular hydrogen bonding between the dipeptide amide groups. Variable-temperature UV–vis studies in apolar MCH show that the supramolecular polymerization of these PDIs proceeds via an isodesmic or weakly cooperative mechanism, resulting in fibrillar supramolecular polymers. Similar results are observed in aqueous media, where the assembly also forms H-type aggregates without evidence of pathway complexity.**

## 1. Introduction

In the field of supramolecular chemistry, supramolecular polymers have emerged as a fascinating class of materials with remarkable mechanical, optical, or biomedical properties.[1] Unlike traditional polymers, whose structure is defined by covalent bonds, supramolecular polymers assemble through the synergy of non-covalent forces. These dynamic interactions allow greater flexibility in material design and enable self-healing, adaptability, and recyclability.[2] A key aspect of the potential function that a supramolecular polymer can exhibit is the mechanism followed by the monomeric units to yield the final supramolecular ensemble. The formation of a large number of supramolecular polymers is dictated by an isodesmic or a cooperative mechanism. In the former, the whole process is controlled by a single binding constant. In the latter, however, two regimes, nucleation and elongation, are identified, each of them defined by the corresponding nucleation and elongation binding constants.[3] The development of mass-balance models has contributed to expanding the knowledge of these thermodynamically controlled supramolecular processes.[4] However, in the last decade, a plethora of kinetically controlled supramolecular polymerizations have been reported. The kinetic control on the supramolecular polymerization often derives from a pathway complexity that yields more than one aggregated species from a single monomeric species.[5] The formation of these aggregated species, which can be interconverted by following a consecutive or a competitive process, usually relies on the appearance of metastable monomeric units that, by subtle changes in concentration, temperature, or solvent composition, can evolve yielding kinetically or thermodynamically controlled supramolecular polymers.[6] A detailed investigation of the mechanism behind some of the supramolecular polymerizations displaying pathway complexity demonstrates that, whilst the kinetically controlled aggregated species follow an isodesmic mechanism, the thermodynamically controlled species are formed by following a cooperative mechanism.[5b,7] Directly related to kinetically controlled supramolecular polymerizations, the seminal works by Aida and coworkers[8] and F. Würthner and coworkers,[9] demonstrated that intramolecularly H-bonded monomers give rise to dormant monomers that strongly condition the kinetics of the supramolecular polymerization and have contributed to the development of the seeded- and living supramolecular polymerization.[10] These programmable strategies allow controlling the length, polydispersity, and sequence

F. Rey-Tarrío, C. Atienza, L. Sánchez
Departamento de Química Orgánica
Facultad de Ciencias Químicas
Universidad Complutense de Madrid
Madrid 28040, Spain
E-mail: lusamar@ucm.es

The ORCID identification number(s) for the author(s) of this article can be found under https://doi.org/10.1002/smll.202504415



**DOI: 10.1002/smll.202504415**

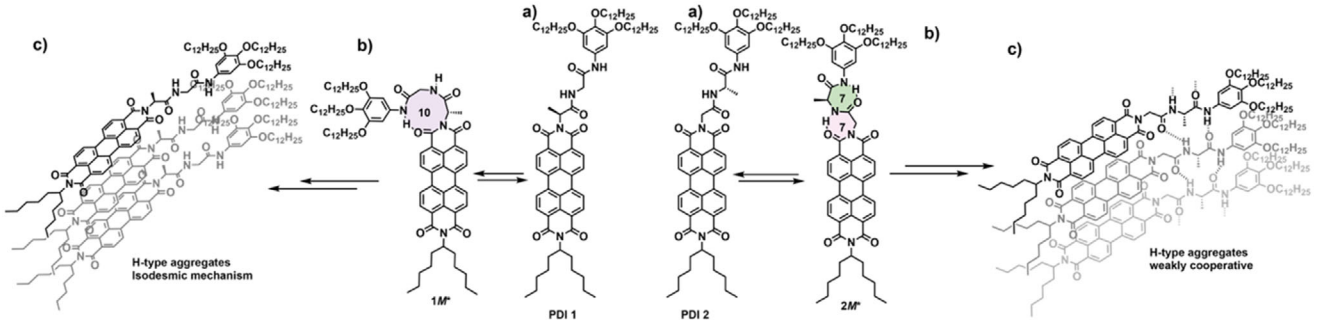


**Figure 1.** The chemical structure of the PDIs endowed with the dipeptide (L)-Ala-Gly (**1**) and Gly-(L)-Ala (**2**) (a); the metastable monomeric species (b) and the H-type aggregates (c).

of the supramolecular polymers constructed by applying these techniques.[5b,7–10]

An elegant and useful strategy to achieve intramolecularly H-bonded metastable monomeric species consists of the decoration of $\pi$-conjugated systems with amino acids. Thus, the presence of peripheral oligopeptides attached to focal $\pi$-conjugated scaffolds is key to attaining efficient catalysts,[11] white-light emitting materials,[12] fuel-driven supramolecular polymerizations[13] and amplification of asymmetry.[14] Importantly, the amide functional groups present in these biomolecules allow the operation of such intramolecular H-bonding interactions that, over time, evolve to intermolecular H-bonding interactions yielding highly organized supramolecular structures. In addition, amino acids (except Gly) present point chirality that can be used to construct chiral supramolecular polymers by the efficient transfer of asymmetry between the monomeric to the aggregated species.[15] Triarylborane,[16] coronene,[17] pyrene[18] are recent examples of such $\pi$-conjugated systems that have been appended with amino acids to give rise to kinetically controlled supramolecular polymers. Especially relevant are perilenediimides (PDIs), a robust and versatile dye that has been extensively studied, functionalized, and applied in different research areas like pigments, organic electronics and to build up chiral, functional supramolecular materials.[19] A key aspect that determines the behavior and final properties of some of these supramolecular polymers is the cooperative mechanism governing the self-assembly process.[16,18] However, examples of kinetically controlled supramolecular polymerizations in which the global mechanism is isodesmic are still scarce.

To address this issue, we present herein the synthesis and self-assembling features of two asymmetrically substituted PDIs, each featuring a peripheral non-polar side chain and a dipeptide moiety: Gly-(*L*)-Ala (compound **1**, **Figure** 1a) or (*L*)-Ala-Gly (compound **2**, Figure 1a). Both asymmetric PDIs **1** and **2** self-assemble straightforwardly in an apolar solvent, such as methylcyclohexane (MCH) or in aqueous media, forming chiral H-type aggregated species. Functionalization of the PDI core with a peptidic sequence promotes the formation of different intramolecularly H-bonded pseudocycles depending on the location of the (*L*)-Ala unit (**1*M**** and **2*M***) (Figure 1b). These metastable monomeric species enable kinetic control over the supramolecular polymerization of the reported PDIs **1** and **2**. However, this kinetic control does not lead to pathway complexity most probably due to the rapid evolution of the active species; instead, only the previously mentioned H-type aggregates are observed. Mechanistic studies conducted using variable temperature (VT) UV–vis spectroscopy reveal that the supramolecular polymerization of **1** and **2** proceeds via an isodesmic or weakly cooperative mechanism (Figure 1c). This mechanism likely precludes the formation of multiple aggregated species from the monomeric PDIs. This study examines the relationship between the supramolecular polymerization mechanism and pathway complexity, emphasizing the interplay between kinetics, structure, and functionality in supramolecular polymers.

## 2. Results and Discussion

### 2.1. Synthesis and Supramolecular Polymerization in Apolar Media

The synthesis of the target PDIs **1** and **2** has been accomplished in a multistep protocol. The dipeptide side chains have been prepared by a sequential synthesis starting from the alkylation of pyrogallol with dodecyl bromide and the subsequent nitration at the 4 position to yield the 1,2,3-tris(dodecyloxy)-5-nitrobenzene **4**. The nitro group of **4** is reduced with hydrazine to afford 3,4,5-tris(dodecyloxy)aniline **5**.[20] The coupling reaction of the corresponding N-Boc protected (*L*)-Ala or Gly with **5** in the presence of EDC, HOBt, and $NEt_3$ gives rise to the amides **6**. The acidic deprotection of the Boc group and the subsequent coupling reaction with the N-Boc protected Gly or (*L*)-Ala yield the N-Boc protected dipeptides **8** that, upon acidic deprotection, afford the deprotected dipeptides **9a**, with a sequence (*L*)-Ala-Gly, or **9b**, with a Gly-(*L*)-Ala sequence (Scheme S1, Supporting Information). On the other hand, 3,4,9,10-perylenetetracarboxylic dianhydride has been utilized as starting material for the aromatic central core. To enhance the processability of the final compounds, the PDI dye has been functionalized with a single undecan-6-amine (**10**) side chain by following a synthetic protocol previously reported in which the *N,N′*-di(1-pentylhexyl)-perylene diimide **11** is first prepared and selectively hydrolyzed with KOH in tert-butanol to yield the monoamide **12**.[21] The final condensation reaction of monoamide **12** with amines **9a-b** in imidazole and $Zn(AcO)_2$ affords the final asymmetric PDIs **1** and **2** (Scheme S1, Supporting Information). All the newly reported compounds have been characterized by applying the standard techniques (see Supporting Information).

 

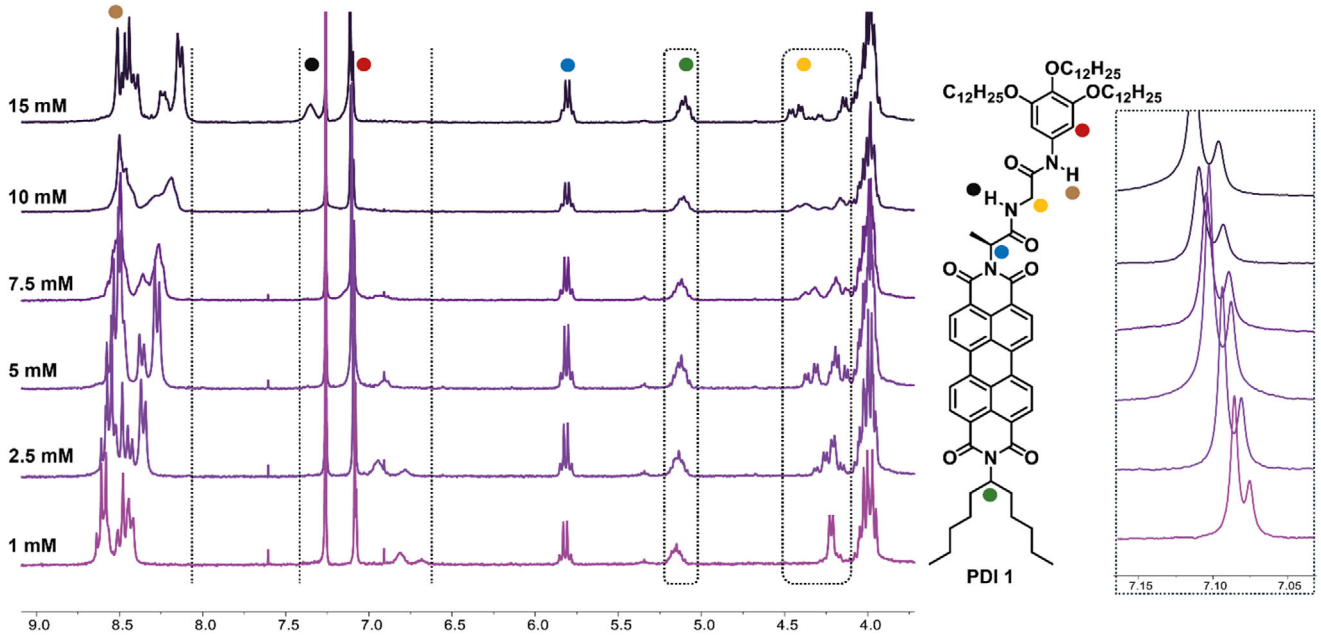


**Figure 2.** Partial $^1$H NMR spectra of PDI **1** at different concentrations showing the aromatic and some of the aliphatic protons. The right part of the figure shows a zoomed view of the singlet ascribable to the protons of the peripheral trialkoxybenzamide fragments ($CDCl_3$, 298 K, 300 MHz).

To investigate the non-covalent interactions involved in the potential self-assembly of the reported PDIs **1** and **2**, we first recorded their $^1$H NMR spectra in $CDCl_3$ at different concentrations. Unexpectedly, the spectra revealed a relatively complex pattern. Considering the symmetry of **1** and **2**, the aromatic region should exhibit a system of four doublets corresponding to the protons of the PDI core. However, a more intricate system is observed, particularly for PDI **1** (**Figure 2**; Figure S10, Supporting Information). Additionally, some signals appear split, such as the singlets at $\delta$~7.1 (attributed to the trialkoxybenzamide moieties) and the resonances at $\delta$~6.5 (assigned to the amide protons) (Figure 2; Figure S10, Supporting Information). The presence of these unexpected resonances, which should theoretically be isochronous, raised the possibility of the formation of different intramolecular pseudocycles due to the structures of the synthesized PDIs. To prove this hypothesis, we recorded the $^1$H NMR spectra of **1** and **2** after adding 10 µL of trifluoroacetic acid (TFA), a reagent that strongly disrupts H-bonding interactions (Figure S11, Supporting Information).[22] Such addition displayed a more simplified resonance pattern of PDIs **1** and **2** in $CDCl_3$. Specifically, the aromatic region showed a simpler arrangement as well as the expected single triplet for the amide group adjacent to the methylene group of Gly in PDI **1** and a doublet for the equivalent amide protons in PDI **2** (black circles in Figure 2; Figure S11a,b, Supporting Information). Moreover, the trialkoxybenzamide moiety exhibited a single singlet for its aromatic protons (red circles in Figure 2; Figure S11a,b, Supporting Information). Notably, the enantiotopic protons of the Gly methylene in PDI **1** showed significant changes. At 1 mM, they appeared as a single doublet, while at higher concentrations (15 mM) in pristine $CDCl_3$, they resolved into two double-doublets (Figure 2). Upon adding TFA to the 1 mM solution, the same double-doublet multiplicity was observed for these enantiotopic protons (yellow circles in Figure 2; Figure S11a, Supporting Information). These results confirm the presence of multiple species of the synthesized PDIs in the good solvent $CDCl_3$. Furthermore, the concentration-dependent $^1$H NMR spectra revealed upfield shifts of the aromatic resonances and deshielding of the amide protons with increasing concentration. This behavior suggests the self-assembly of the PDIs is driven by the $\pi$-stacking of the aromatic cores and the intermolecular H-bonding interactions between the amides (Figure 1c).

The incorporation of amino acids in the side chains of scaffolds capable of undergoing supramolecular polymerization has been reported to form metastable monomeric species ***M****, which, in turn, induces kinetic control.[16,18] To assess the formation of such metastable monomeric species, we first recorded the FTIR spectra of PDIs **1** and **2** in $CHCl_3$ and MCH. In $CHCl_3$, a good solvent that promotes solvation of the PDIs and stabilizes monomeric species,[23] two NH stretching bands appear at 3463 and 3367 $cm^{-1}$ for PDI **1**, values previously associated with free NH groups and intramolecularly H-bonded species, respectively (Figure S12a, Supporting Information; Figure 1a,b).[9,24] For PDI **2**, a weak band is observed at 3455 $cm^{-1}$, attributable to free NH groups, while a more intense band at 3408 $cm^{-1}$, corresponding to intramolecularly H-bonded species, is also visualized (Figure S12b, Supporting Information). In MCH, a poor solvent that strongly favors the self-assembly of PDIs, the NH stretching bands shift to 3321 and 3280 $cm^{-1}$ for PDIs **1** and **2**, respectively. These values are characteristic of intermolecularly H-bonded amides (Figure S12a,b, Supporting Information).[9,24]

Further evidence supporting the formation of metastable monomeric species 1*M** and 2*M** was obtained from VT-$^1$H NMR experiments in $CDCl_3$ at diluted conditions (total concentration, $cT$ = 1 mM). For both PDIs **1** and **2**, increasing the temperature did not produce significant changes in the chemical

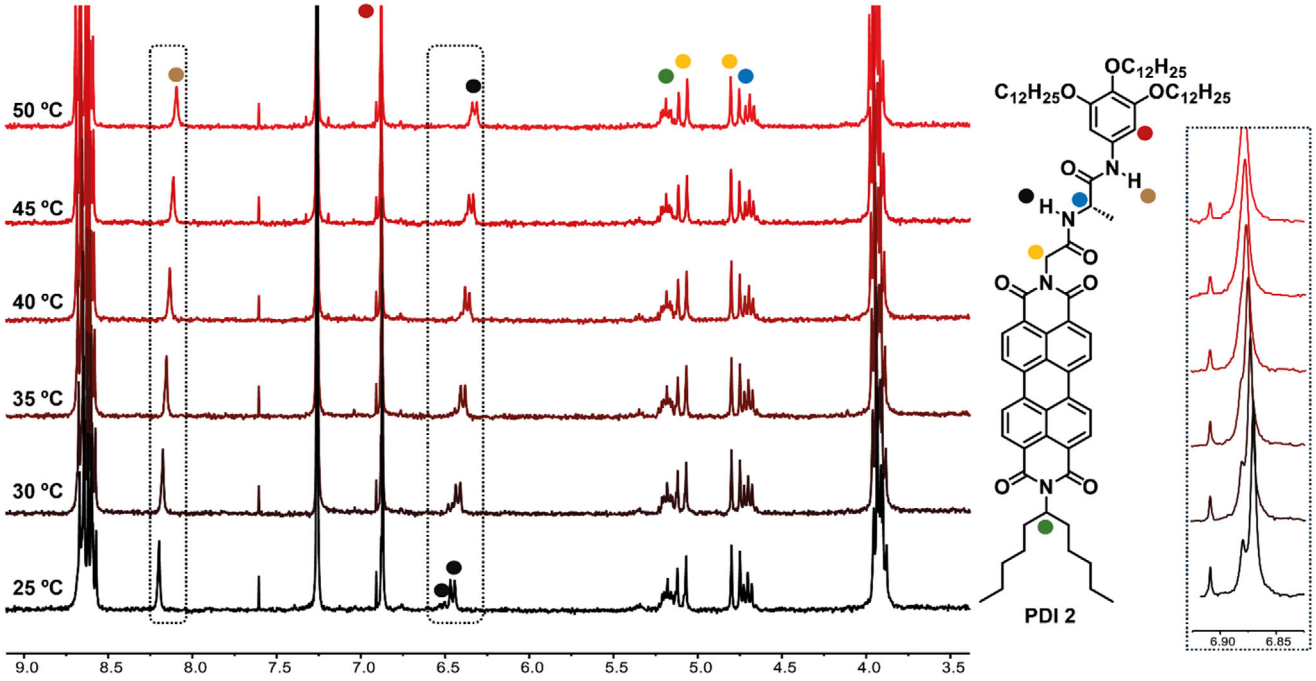


**Figure 3.** Partial $^{1}$H NMR spectra of PDI **2** at different temperatures showing the aromatic and some of the aliphatic protons. The right part of the figure shows a zoomed view of the singlet ascribable to the protons of the peripheral trialkoxybenzamide fragments ($CDCl_3$, 300 MHz, $c_T$ = 1mM).

shifts of the aromatic resonances and most of the aliphatic protons (**Figure 3**; Figure S13, Supporting Information). However, the resonances associated with the amide functional groups exhibited upfield shifts with increasing temperature, indicating the disruption of intramolecular H-bonding interactions. Interestingly, the presence of multiple resonances for the amide protons near the (*L*)-Ala fragment (blue circles in Figure 3; Figure S13, Supporting Information) suggests the existence of different conformations in the metastable, intramolecularly H-bonded monomers ***M****.[24] This conformational variability is further supported by the shifting of aromatic resonances of the peripheral trialkoxybenzamide units (red circles in Figure 3; Figure S13, Supporting Information), corroborating the dynamic interconversion between different monomeric conformations.

To further explore the most stable conformations of the metastable monomeric species ***1M**** and ***2M****, we performed DFT theoretical calculations at the B3LYP/6-31G** level, replacing the peripheral dodecyloxy side chains with methoxy groups. The substitution facilitates modeling while preserving the key structural and electronic features of the central PDI core, which is decorated with an (*L*)-Ala-Gly linker for **1** and a Gly-(*L*)-Ala linker for **2**.[25] This configuration allows for the construction of fully unbonded monomers (**1*M**I** and **2*M**I, Figure 4**) as well as various metastable monomeric species stabilized by intramolecular H-bonding interactions. For PDI **1**, several conformations were computed, with the most stable being **1*M**II**, characterized by the formation of a 10-membered pseudocycle between the NH group of the outer Gly and one of the carbonyl groups of the central imide (Figures 4b and 1b; Figure S14a, Supporting Information). Close in energy is the conformer **1*M**III**, which features two 7-membered pseudocycles: one formed between the NH of Gly and the carbonyl of (*L*)-Ala, and the other between the NH of (*L*)-Ala and one of the PDI core carbonyls (Figure 4c; Figure S14b, Supporting Information). Additionally, the fully unbonded conformer **1*M**I**, which lacks intramolecular H-bonds (Figure 4a), is also energetically comparable. These three conformations are sufficiently close in energy to coexist under the experimental conditions described. It is worth noting that conformers where only a single 7-membered pseudocycle is formed (**1*M**IV** and **1*M**V** in Figure 4d,e; Figure S14c,d, Supporting Information) are slightly less stable. However, the small energy differences suggest that these species may also coexist as metastable intermediates. In all the computed metastable monomeric species, the intramolecular H-bonding interactions exhibit a bond distance of ≈2 Å (Figure 4; Figure S14, Supporting Information).

For PDI **2**, the most stable conformation of the metastable monomeric species is **2*M**II**, characterized by the formation of two intramolecular H-bonding interactions (Figures 1b and 4g; Figure S14e, Supporting Information). The first H-bond is established between the NH group of the outer (*L*)-Ala and the carbonyl of the Gly unit, while the second forms between the NH of the Gly and one of the carbonyls of the PDI core (Figures 1b and 4g; Figure S14e, Supporting Information). Notably, the completely unbonded monomeric species (**2*M**I**, Figure 4f) is very close in energy, with a difference of only 7.6 kJ mol$^{-1}$. This small energy difference is also observed in other intramolecularly H-bonded conformers. For instance, in **2*M**III** (Figure 4h; Figure S14f, Supporting Information), a single 7-membered, pseudocycle is formed between the NH of the outer (*L*)-Ala and the carbonyl of the Gly. Similarly, **2*M**IV** (Figure 4i; Figure S14g, Supporting Information) features a 10-membered pseudocycle formed between the NH of (*L*)-Ala and one of the carbonyls of the PDI core, while **2*M**V** (Figure 4j; Figure S14h, Supporting Information) presents a 7-membered pseudocycle formed between

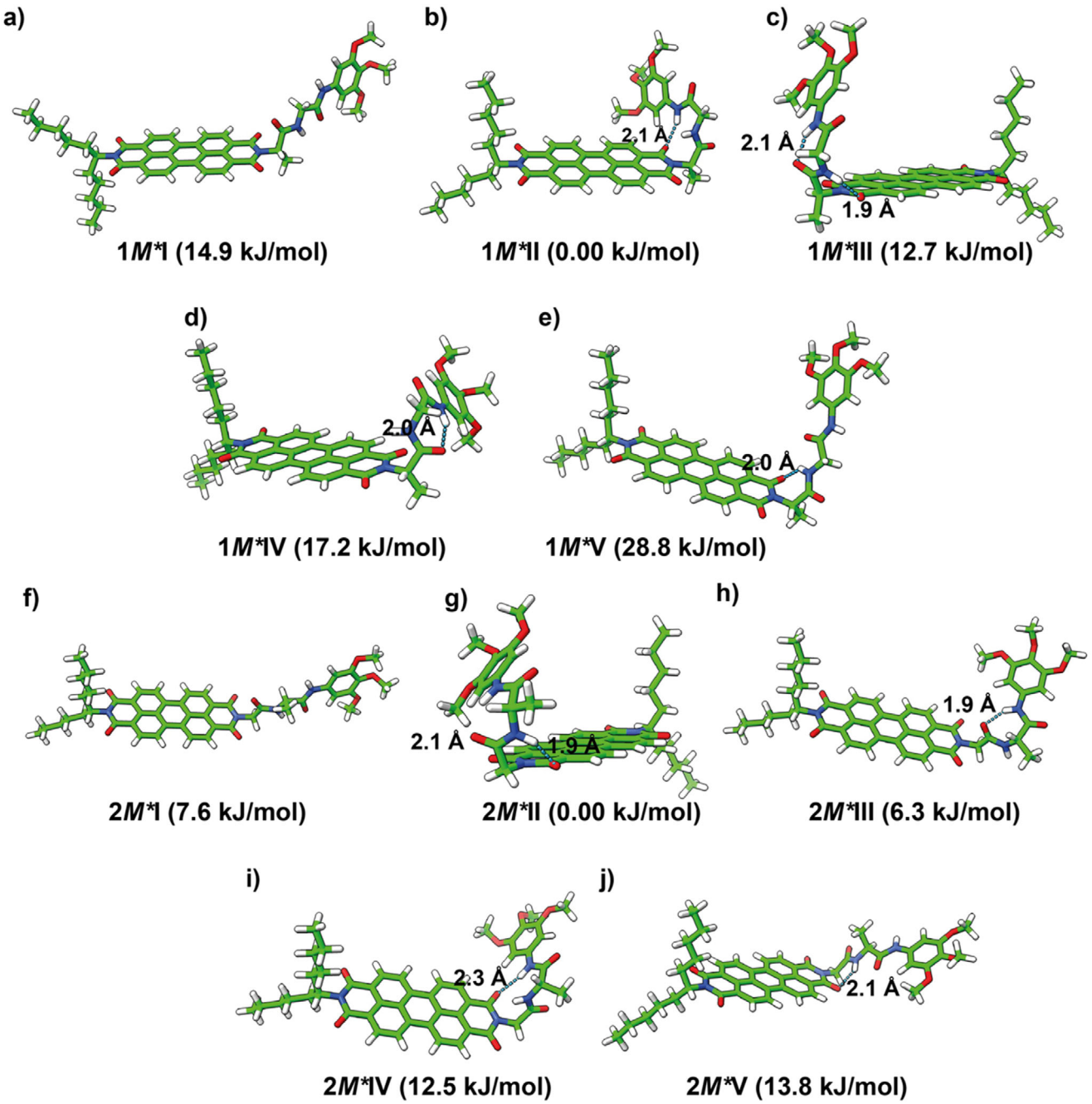


**Figure 4.** Minimum-energy structures (with their relative energy indicated) computed at the B3LYP/6-31G** level for the most stable conformers of monomers of PDI **1** (a–e) and PDI **2** (f–j). The intramolecular H-bonding interactions are depicted in black.

the NH of the inner Gly and one of the carbonyls of the PDI core. In all these metastable monomeric species, the intramolecular H-bond distances are ≈2 Å. The minimal energetic differences among these conformers suggest that they exhibit similar stabilities, allowing them to coexist under the experimental conditions explored in the solution.

After experimentally and theoretically investigating the formation and stability of the metastable monomeric species, we proceeded to study the supramolecular polymerization of the reported PDIs **1** and **2**. Guided by previous studies on scaffolds incorporating amino acids,[16–18] we conducted VT-UV–vis experiments using MCH as the solvent. At highly diluted conditions ($c_T$ = 10 μM) and at 90 °C, the UV–vis spectra of both PDIs display the characteristic $A_{n-1}/A_{n-n}$ transitions with maxima at $\lambda$ = 516 and 481 nm, accompanied by a shoulder at 451 nm (**Figure** 5a,b).[26] This absorption pattern matches the spectra recorded for PDIs **1** and **2** in $CHCl_3$, confirming the presence of monomeric species in MCH at high temperatures (Figure S15, Supporting Information). In contrast, at 20 °C, the UV–vis spectra in MCH show a pronounced hypochromic effect, with

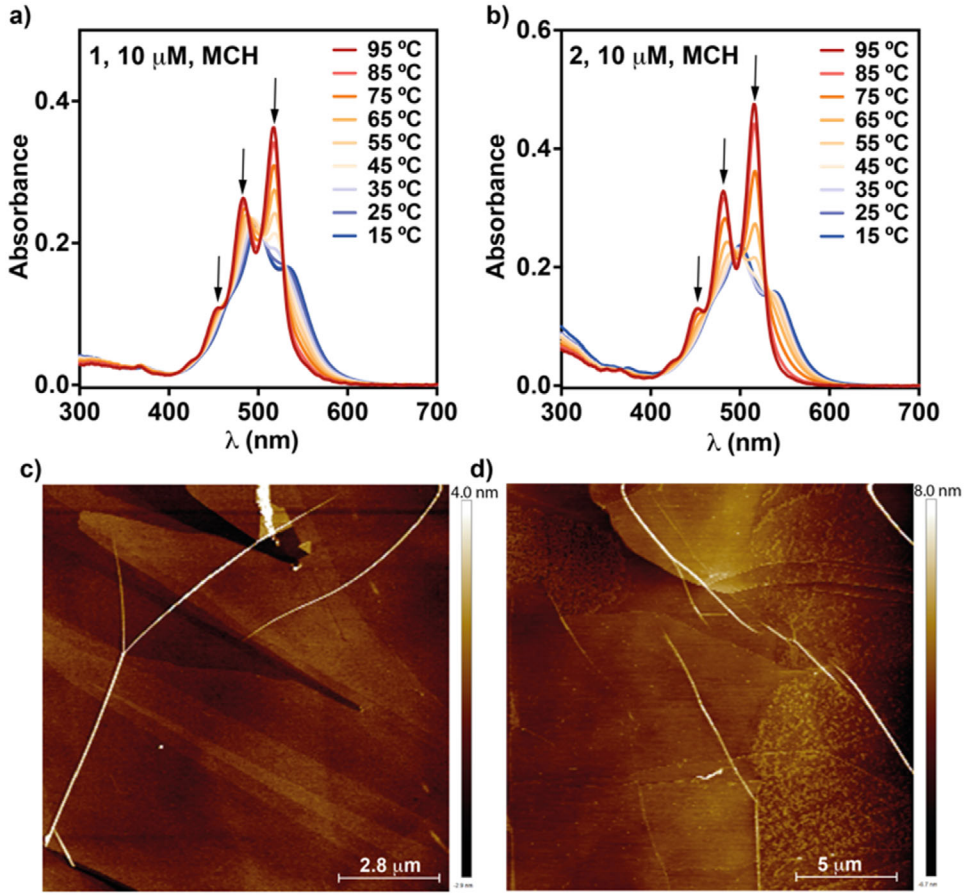


**Figure 5.** a,b) UV–vis spectra of **1** (a) and **2** (b) in MCH at different temperatures ($c_T$ = 10 μM). Arrows indicate the changes observed in the absorption pattern upon decreasing the temperature. c,d) Height AFM images of the fibrillar aggregates formed by **1** (c) and **2** (d) onto HOPG (MCH, $c_T$ = 10 μM; z scale 4 and 8 nm for panels (c) and (d) respectively).

absorption maxima shifting to $\lambda$ = 533 and 495 nm (Figure 5a,b; Figure S15, Supporting Information). These spectral changes are indicative of the formation of H-type aggregates, in which the PDI units adopt a cofacial arrangement.[27] The formation of such aggregates was further corroborated by recording the emission spectra in MCH, $CHCl_3$ and MCH/$CHCl_3$ mixtures, where the ratio of the good solvent ($CHCl_3$) and the poor solvent (MCH) varied while maintaining constant the total concentration. The photoluminescence maxima at $\lambda$ = 537, 578 and 625 nm decrease significantly upon increasing the proportion of MCH (Figure S16a,b, Supporting Information). Moreover, while the color of solutions of PDIs **1** and **2** in MCH and $CHCl_3$ appears similar, their fluorescence behavior changes dramatically upon irradiation, as evidenced by the distinct color shifts in these solutions (Figure S16c–f, Supporting Information). This aggregation-caused quenching (ACQ) effect provides additional confirmation of the formation of the aforementioned H-type aggregates (Figure S16, Supporting Information).[27] The formation of supramolecular polymers from **1** and **2** is further corroborated by registering the corresponding CD spectra in MCH. We have initially registered the CD spectra of **1** and **2** by using a total concentration of 10 μM. The CD spectra of these two PDIs endowed with the aminoacid residues appeared very weak in comparison to many other PDI-based supramolecular polymers in which the aromatic scaffold is not decorated with amino acid residues (Figure S17a, Supporting Information).[28] To further investigate the transfer of asymmetry from the chiral Ala residue to the final supramolecular polymer, we have increased the concentration of the measured solution to $c_T$ = 50 μM. In these experimental conditions, both PDIs display an intense dichroic response and a −/+ bisignated pattern, with maxima at $\lambda \sim$ 540 and 485 nm, two shoulders at $\lambda \sim$ 514 and 461 nm, and a zero-crossing point at $\lambda$ = 513 nm, diagnostic of the formation of *M*-type helical structures due to the efficient transfer of asymmetry from the point chirality embedded in the (*L*)-Ala unit located at the central linker (Figure S17b, Supporting Information).[14,29] To investigate the thermal stability of the supramolecular polymers formed by **1** and **2** in MCH we heated up the MCH solutions to 95 °C to favor the complete disassembly. However, the CD response is not canceled even decreasing the concentration to $c_T$ = 25 μM, diagnostic of the high stability of the aggregated species (Figure S17c, Supporting Information).

To evaluate the influence of the metastable monomeric species ***M**** on the supramolecular polymerization of PDIs **1** and **2**, we recorded cooling and heating curves in MCH solutions at various concentrations, applying a cooling and heating rate of

**Table 1.** Thermodynamic parameters associated with the supramolecular polymerization of PDIs **1** and **2** in MCH.

| | $\Delta H_e$ [a)] | $\Delta H_n$ [a)] | $\Delta S$ [b)] | $\Delta G$ [a)] | $K_e$ [c)] | $K_n$ [c)] |
|---|---|---|---|---|---|---|
| **1** | −286.9 ± 1 | 0 | −166 ± 3 | −32.1 | 5,3 e5 | |
| **2** | −73.5 ± 1 | −10.8 ± 1 | −114 ± 4 | −33.9 | 8,7e6 | 1,8e5 |

[a)] kJ $mol^{-1}$; [b)] J $Kmol^{-1}$; [c)] $M^{-1}$.

1 °C $min^{-1}$. Surprisingly, these cycles exhibited negligible hysteresis, effectively ruling out a kinetically controlled supramolecular polymerization for both compounds (Figure S18, Supporting Information).[9,10] To further confirm the thermodynamic nature of the polymerization process, we repeated the experiments using a slower rate of 0.1 °C $min^{-1}$. Once again, the absence of hysteresis in the cooling and heating curves corroborates that the supramolecular polymerization of PDIs **1** and **2** is thermodynamically controlled (Figure S19, Supporting Information). Moreover, the sigmoidal shape of these curves is characteristic of an isodesmic supramolecular polymerization mechanism, defined by a single binding constant.[3] A global fit of the cooling curves at various concentrations and a rate of 1 °C $min^{-1}$ was performed using the one-component equilibrium (EQ) model (Figure S20, Supporting Information).[30] The resulting thermodynamic parameters for the supramolecular polymerization of PDIs **1** and **2** are summarized in **Table 1**. For PDI **1**, the polymerization follows an isodesmic mechanism with a binding constant $K_e = 5.3 \times 10^5$ $M^{-1}$ (Table 1). In contrast, PDI **2** exhibits weak cooperativity ($\sigma = K_n/K_e = 0.01$, Table 1), with nucleation and elongation binding constants of comparable magnitude.

Noteworthy, the cooling curves utilized for deriving the thermodynamic parameter present no clear saturation at high temperatures despite the clear absorption pattern observed in these conditions ascribable to the monomeric species. To further corroborate the accuracy of this analysis, we have also performed a solvent denaturation (SD) experiment for both PDIs **1** and **2**. In these experiments, two solutions of the studied PDIs at $c_T$ = 10 μM in the poor solvent MCH, which favors the self-assembly, and in the good solvent $CHCl_3$, which favors the disassembly, are mixed at different ratios. As expected, the addition of increasing amounts of the $CHCl_3$ solution provokes a gradual disassembly, as demonstrated by the corresponding absorption pattern of the resulting mixtures (Figure S21a,b, Supporting Information). Plotting the variation of the degree of aggregation, calculated from the variation of the absorbance at $\lambda$ = 529 nm,[28] versus the molar fraction of the good solvent yields sigmoidal curves diagnostic of isodesmic mechanism (Figure S21c,d, Supporting Information). In fact, fitting these sigmoidal curves to the SD model reported by Meijer and coworkers[23] affords a degree of cooperativity $\sigma$ = 1, as expected for an isodesmic mechanism (Table S1, Supporting Information). Additionally, this SD model provides the value of the free Gibbs energy released that is very similar for both PDIs **1** and **2** (Table S1, Supporting Information).

Finally, we have visualized the morphology of the supramolecular polymers formed by **1** and **2** by registering atomic force microscopy (AFM) images and by using highly oriented pyrolytic graphite (HOPG) as a surface. The spin-coating of diluted solutions of **1** and **2** in MCH ($c_T$ = 10 μM) onto HOPG shows the formation of long, rope-like fibrillar aggregates of several micrometers in length (Figure 5c,d; Figures S22 and S23, Supporting Information). The height profiles of the fibrillar aggregates formed by **1** is of 2.5 and 6 nm. The former roughly corresponds to the length of the reported PDIs along the large axis. In the former, the larger height is diagnostic of the intertwining of thinner fibers (Figures S22 and S23a, Supporting Information). PDI **2** forms thinner fibers of ≈3 nm diagnostic of the formation of unimolecular columnar stacks (Figures S23b and S24, Supporting Information).

### 2.2. Self-Assembly in Aqueous Media

The functionalization of self-assembling scaffolds with amino acids or peptides provides a versatile strategy to introduce pathway complexity in aqueous environments. Recent studies highlight the profound impact of the aqueous medium on the formation of aggregates with diverse morphologies, such as nanoparticles or helical structures, derived from amino acid-based systems.[17,19] In particular, the presence of the (*L*)-Ala-Gly or Gly-(*L*)-Ala dipeptides in amphiphilic PDIs **1** and **2**, respectively, motivated an investigation into their self-assembly properties in aqueous media.

To deepen this analysis, solvent denaturation (SD) experiments were performed using THF as a good solvent and $H_2O$ as a poor solvent. In these experiments, solutions of PDIs **1** and **2** at different THF/$H_2O$ ratios, but with constant total concentration, were mixed to facilitate self-assembly.[23] It is noteworthy that both PDIs exhibit limited solubility in pure water, prompting the initial studies to employ a THF/$H_2O$ 9:1 mixture where the systems are fully aggregated (**Figure 6**; Figure S23, Supporting Information). For PDI **1**, the absorption spectrum in the THF/$H_2O$ 9:1 mixture mirrors the pattern observed in MCH, with maxima at $\lambda$ = 537 and 498 nm, ascribable to the formation of H-type aggregates (Figure 6a). Conversely, in pristine THF, the absorption spectrum displays the characteristic monomeric PDI transitions, with maxima at $\lambda$ = 523 and 488 nm, accompanied by a shoulder at 458 nm (Figure 6a).[26] The progressive addition of water induces the formation of such H-type aggregated species, which is complete at a 40:60 THF/$H_2O$ ratio (Figure 6a). Importantly, these SD studies with PDI **1** reveal no evidence of new aggregated species, and no kinetic effects are observed, as the absorption pattern remains unchanged after 24 h of sample aging (Figure S25a, Supporting Information). For PDI **2**, the SD experiments display analogous results for its supramolecular polymerization in aqueous media, ultimately leading to the formation of H-type aggregated species. The progressive self-assembly from monomeric to aggregated species is evidenced by the hypochromic effect in the absorption spectrum (Figure 6b). Similarly to PDI **1**, no changes in the absorption pattern are observed after 24 h of

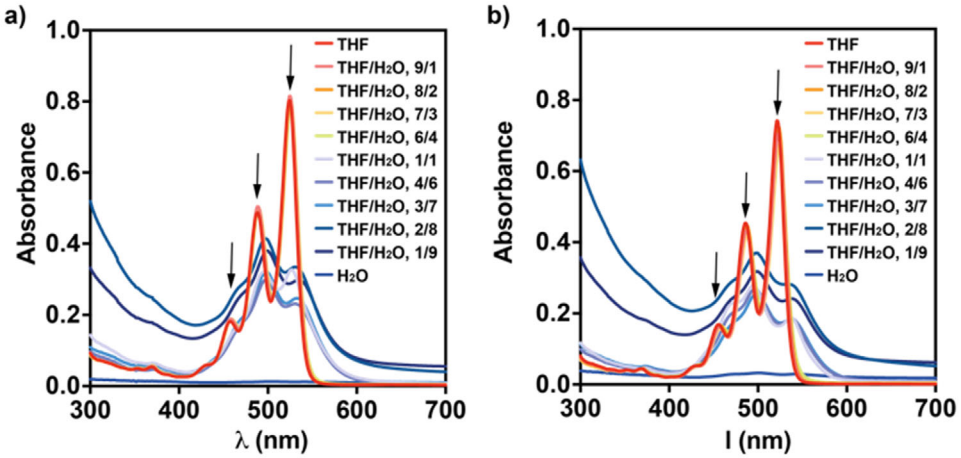


**Figure 6.** a,b) UV–vis spectra of **1** (a) and **2** (b) in THF/$H_2O$ mixtures (20 °C; $c_T$ = 10 μM). Arrows indicate the changes observed in the absorption pattern upon increasing the ratio of $H_2O$.

aging (Figure S25b, Supporting Information). Therefore, the self-assembly behavior of PDIs **1** and **2** in aqueous media does not exhibit pathway complexity, as both compounds follow a similar aggregation mechanism, culminating in the formation of H-type aggregates.

## 3. Conclusion

In summary, we report the synthesis of two amphiphilic PDI-based systems, each featuring lateral non-polar side chains and dipeptide residues: (*L*)-Ala-Gly (PDI **1**) or Gly-(*L*)-Ala (PDI **2**). The amphiphilic nature of these dipeptides enables the exploration of their self-assembling properties in both apolar (MCH) and aqueous media. Functionalization with dipeptide residues promotes the formation of metastable monomeric species, M*, which have been studied experimentally and theoretically. Spectroscopic analyses of the monomeric species reveal the presence of various configurations stabilized by intramolecular hydrogen bonding, leading to pseudocycles of differing sizes. DFT calculations indicate that these metastable monomers and their fully unbonded counterparts exhibit comparable stabilities, allowing their coexistence in solution. Surprisingly, and in contrast to previous reports on amino acid-based scaffolds, the presence of these metastable species does not result in pathway complexity. Instead, a single H-type aggregate species is formed through $\pi$-stacking of the PDI cores and intermolecular hydrogen bonding between the amide groups of the dipeptide residues. Remarkably, variable-temperature UV–vis studies conducted in apolar MCH demonstrate that the supramolecular polymerization of these PDIs follows an isodesmic or weakly cooperative mechanism, resulting in fibrillar supramolecular polymers. Identical behavior is observed in aqueous media, where the self-assembly process also yields H-type aggregates without pathway complexity. The findings presented here advance our understanding of the structural complexity achievable by metastable monomeric species while highlighting the relatively simple self-assembly process that produces supramolecular polymers from optically active scaffolds.

## Supporting Information

Supporting Information is available from the Wiley Online Library or from the author.

## Acknowledgements

Financial support by the MCIN/AEI of Spain (PID2023-146971NB-I00 and TED2021-130285B-I00) was acknowledged.

## Conflict of Interest

The authors declare no conflict of interest.

## Data Availability Statement

The data that supports the findings of this study have been included in the main text and supporting information (SI) and are available from the corresponding authors upon reasonable request.

## Keywords

amphiphiles, dipeptides, kinetics, perilediimides, supramolecular polymers

Received: April 9, 2025
Revised: May 19, 2025
Published online:

[1] a) T. Aida, E. W. Meijer, S. I. Stupp, *Science* **2012**, *335*, 813; b) W. Zhao, J. Tropp, B. Qiao, M. Pink, J. D. Azoulay, A. H. Flood, *J. Am. Chem. Soc.* **2020**, *142*, 2579; c) Z. Álvarez, A. N. Kolberg-Edelbrock, I. R. Sasselli, J. A. Ortega, R. Qiu, Z. Syrgiannis, P. A. Mirau, F. Chen, S. M. Chin, S. Weigand, E. Kiskinis, S. I. Stupp, *Science* **2021**, *374*, 848; d) O. Dumele, L. Đorđević, H. Sai, T. J. Cotey, M. H. Sangji, K. Sato, A. J. Dannenhoffer, S. I. Stupp, *J. Am. Chem. Soc.* **2022**, *144*, 3127.

[2] L. Brunsveld, B. J. B. Folmer, E. W. Meijer, R. P. Sijbesma, *Chem. Rev.* **2001**, *101*, 4071.
[3] T. F. A. De Greef, M. M. J. Smulders, M. Wolffs, A. P. H. J. Schenning, R. P. Sijbesma, E. W. Meijer, *Chem. Rev.* **2009**, *109*, 5687.
[4] H. M. M. ten Eikelder, A. J. Markvoort, *Acc. Chem. Res.* **2019**, *52*, 3465.
[5] a) P. A. Korevaar, S. J. George, A. J. Markvoort, M. M. J. Smulders, P. A. J. Hilbers, A. P. H. J. Schenning, T. F. A. De Greef, E. W. Meijer, *Nature* **2012**, *481*, 492; b) S. Ogi, K. Sugiyasu, S. Manna, S. Samitsu, M. Takeuchi, *Nat. Chem.* **2014**, *6*, 188.
[6] a) S. Dhiman, S. J. George, *Bull. Chem. Soc. Jpn.* **2018**, *91*, 687; b) J. Matern, Y. Dorca, L. Sánchez, G. Fernández, *Angew. Chem., Int. Ed.* **2019**, *58*, 16730; c) M. Wehner, F. Würthner, *Nat. Chem. Rev.* **2019**, *4*, 38.
[7] a) S. Ogi, T. Fukui, M. L. Jue, M. Takeuchi, K. Sugiyasu, *Angew. Chem., Int. Ed.* **2014**, *53*, 14363; b) D. van der Zwaag, P. A. Pieters, P. A. Korevaar, A. J. Markvoort, A. J. H. Spiering, T. F. A. de Greef, E. W. Meijer, *J. Am. Chem. Soc.* **2015**, *137*, 12677; c) A. T. Haedler, S. C. J. Meskers, R. H. Zha, M. Kivala, H. Schmidt, E. W. Meijer, *J. Am. Chem. Soc.* **2016**, *138*, 10539; d) T. Fukui, S. Kawai, S. Fujinuma, Y. Matsushita, T. Yasuda, T. Sakurai, S. Seki, M. Takeuchi, K. Sugiyasu, *Nat. Chem.* **2017**, *9*, 493; e) M. F. J. Mabesoone, A. J. Markvoort, M. Banno, T. Yamaguchi, F. Helmich, Y. Naito, E. Yashima, A. R. A. Palmans, E. W. Meijer, *J. Am. Chem. Soc.* **2018**, *140*, 7810.
[8] J. Kang, D. Miyajima, T. Mori, T. Inoue, Y. Itoh, T. Aida, *Science* **2015**, *347*, 646.
[9] a) S. Ogi, V. Stepanenko, K. Sugiyasu, M. Takeuchi, F. Würthner, *J. Am. Chem. Soc.* **2015**, *137*, 3300; b) S. Ogi, V. Stepanenko, J. Thein, F. Würthner, *J. Am. Chem. Soc.* **2016**, *138*, 670.
[10] a) C. Naranjo, S. Adalid, R. Gómez, L. Sánchez, *Angew. Chem., Int. Ed.* **2024**, *62*, 202218572; b) H. Wang, Y. Zhang, Y. Chen, H. Pan, X. Ren, Z. Chen, *Angew. Chem., Int. Ed.* **2020**, *59*, 5185; c) A. Chakraborty, G. Ghosh, D. S. Pal, S. Varghese, S. Ghosh, *Chem. Sci.* **2019**, *10*, 7345.
[11] K. S. Lee, J. R. Parquette, *Chem. Commun.* **2015**, *51*, 15653.
[12] a) H. A. M. Ardoña, J. D. Tovar, *Chem. Sci.* **2015**, *6*, 1474; b) M. K. Manna, D. B. Rasale, A. K Das, *RSC Adv.* **2015**, *5*, 90158.
[13] A. Sorrenti, A. Leira-Iglesias, A. Sato, T. M. Hermans, *Nat. Comm.* **2017**, *8*, 15899.
[14] T. Pal, S. Samanta, D. Chaudhuri, *ACS Nano* **2024**, *18*, 11349.
[15] F. García, R. Gómez, L. Sánchez, *Chem. Soc. Rev.* **2023**, *52*, 7524.
[16] H. Choi, S. Ogi, N. Ando, S. Yamaguchi, *J. Am. Chem. Soc.* **2021**, *143*, 2953.
[17] a) D. Elizebath, J. H. Lim, Y. Nishiyama, B. Vedhanarayanan, A. Saeki, Y. Ogawa, V. K Praveen, *Small* **2023**, *20*, 2306175; b) D. Elizebath, S. Sharma, S. Varughese, C. N. Ramachandran, V. K Praveen, *Small* **2024**, *21*, 2405305.
[18] a) S. Ogi, K. Matsumoto, S. Yamaguchi, *Angew. Chem., Int. Ed.* **2018**, *57*, 2339; b) K. Matsumoto, N. Bäumer, S. Ogi, S. Yamaguchi, *Angew. Chem., Int. Ed.* **2024**, *63*, 202416361.
[19] a) C. Kaufmann, W. Kim, A. Nowak-Król, Y. Hong, D. Kim, F. Würthner, *J. Am. Chem. Soc.* **2018**, *140*, 4253; b) J. Han, S. Fujikawa, N. Kimizuka, *Angew. Chem., Int. Ed.* **2024**, *63*, 202410431.
[20] V. Percec, E. Aqad, M. Peterc, J. G. Rudick, L. Lemon, J. C. Ronda, B. B. De Paul, A. Heiney, E. W. Meijer, *J. Am. Chem. Soc.* **2006**, *128*, 16365.
[21] Y. Hu, S. Chen, L. Zhang, Y. Zhang, Z. Yuan, X. Zhao, Y. Chen, *J. Org. Chem.* **2017**, *82*, 5926.
[22] H. Su, S. A. H. Jansen, T. Schnitzer, E. Weyandt, A. T. Rösch, J. Liu, G. Vantomme, E. W. Meijer, *J. Am. Chem. Soc.* **2021**, *143*, 17128.
[23] P. A. Korevaar, C. Schaefer, T. F. A. de Greef, E. W. Meijer, *J. Am. Chem. Soc.* **2012**, *134*, 13482.
[24] a) M. Wehner, M. I. S. Röhr, M. Böhler, V. Stepanenko, W. Wagner, F. Würthner, *J. Am. Chem. Soc.* **2019**, *141*, 6092; b) E. E. Greciano, J. Calbo, E. Ortí, L. Sánchez, *Angew. Chem., Int. Ed.* **2020**, *59*, 17517; c) C. Naranjo, S. Adalid, R. Gómez, L. Sánchez, *Angew. Chem., Int. Ed.* **2023**, *62*, 202218572.
[25] F. Rey-Tarrío, L. Sánchez, *Angew. Chem., Int. Ed.* **2025**, *64*, 202418301.
[26] F. Würthner, C. R. Saha-Möller, B. Fimmel, S. Ogi, P. Leowanawat, D. Schmidt, *Chem. Soc. Rev.* **2016**, *116*, 962.
[27] F. Würthner, T. E. Kaiser, C. R. Saha-Möller, *Angew. Chem., Int. Ed.* **2011**, *50*, 3376.
[28] S. Ghosh, X. Li, V. Stepanenko, F. Würthner, *Chem. - Eur. J.* **2008**, *14*, 11343.
[29] N. S. S. Nizar, M. Sujith, K. Swathi, C. Sissa, C. Painelli, K. G. Thomas, *Chem. Soc. Rev.* **2021**, *50*, 11208.
[30] H. M. M. ten Eikelder, A. J. Markvoort, T. F. A. de Greef, P. A. J. Hilbers, *J. Phys. Chem. B* **2012**, *116*, 5291.